JSEE Vol. 27, No. 3, 2025 DOI: 10.48303/jsee.2024.2018297.1084

Research Paper

Investigating the Effect of Steel Ring Damper on the Seismic Performance of Concrete Frames by Numerical Method

Kambiz Cheraghi[1], Hamed Mahdiani[2], Omid Rezaeichaghabalaki[1] and Mohammad Hadi Tavana[3*]

1. M.Sc. of Structural Engineering, Department of Civil Engineering, Razi University, Kermanshah, Iran
2. M.Sc. of Structural Engineering, Department of Civil Engineering, Ker. C., Islamic Azad University, Kermanshah, Iran
3. Assistant Professor, Department of Civil Engineering, Ker. C., Islamic Azad University, Kermanshah, Iran,
*Corresponding Author; email: m.h.tavana@iau.ac.ir

Received: 20/12/2023
Revised: 11/08/2024
Accepted: 28/08/2024

Keywords:
Steel ring damper, Energy dissipation, RC frame, Numerical Analysis, Push-over analysis

ABSTRACT

Steel ring dampers are a type of yielding damper that has a good energy dissipation capability. In this research, parametric studies were conducted to investigate the influence of the radius and thickness of the steel ring damper (SRD) on the seismic behavior of the RC frame. The numerical model was first calibrated with two experimental samples, and then the impact of the damper on the concrete frame was investigated by performing a pushover analysis. Simplified two-line curves were then obtained to calculate the seismic parameters of the frame, including stiffness, strength, ductility, and energy dissipation parameters. To estimate the elastic stiffness and ultimate strength of the SRD-equipped concrete frame, approximate equations were presented, which agreed well with the numerical results. In addition, the dynamic behavior of the SRD-equipped frame was investigated under seven earthquakes. The results showed that reducing the radius of the damper and increasing its thickness increases the stiffness and strength of the frame. Also, increasing the thickness of the damper increases the energy dissipation and reduces the ductility of the frame. It was also observed that if the stiffness ratio of the damper to the bare frame is set to 4.1, the energy dissipation and ductility of the RC frame will be two times that of the bare frame.

How to cite the article:
Cheraghi, K., Mahdiani, H., Rezaeichaghabalaki, O. & Tavana, M. H. (2025). Investigating the effect of steel ring damper on the seismic performance of concrete frames by numerical method. *Journal of Seismology and Earthquake Engineering*, 27(3), 29-43, https://doi.org/10.48303/jsee.2024.2018297.1084

Copyright © 2024 IIEES. Published by International Institute of Earthquake Engineering and Seismology.
This work is licensed under a Creative Commons Attribution-NonCommercial 4.0 International license (https://creativecommons.org/licenses/by-nc/4.0/). Non-commercial uses of the work are permitted, provided the original work is properly cited.

1. Introduction

Yielding dampers serve as an effective means to enhance the seismic resilience of buildings. These dampers undergo yielding when subjected to deformation, effectively absorbing a portion of the energy transmitted through the structure (Hosseini Hashemi & Keykhosrokiany, 2019; Sedaghatnezhad et al., 2021; Cheraghi et al., 2023d, 2023c, 2023a). In addition to increasing energy dissipation, these dampers also improve the stiffness and strength of the structure, making them a practical choice for retrofitting moment-resisting frames (Zahrai & Heisami, 2017; Zahrai & Parsa, 2015).

In recent years, there have been multiple proposals for yielding dampers for retrofitting concrete and steel frames. Bagheria et al. (2011) highlighted the importance of design parameters in metallic-yielding dampers for reducing dynamic responses in buildings. They found that a fixed B/D ratio for all stories does not ensure uniform distribution of ductility and optimized damper usage. By implementing a method based on uniform deformation distribution, they demonstrated that different B/D ratios are needed for optimal dynamic behavior, with higher ratios in upper stories and lower ratios in lower stories. Mahmoudi et al. (2019) proposed a shear link at the mid-span of beams to address conflicts between seismic codes and the need for shorter spans in tall buildings. Experimental results showed satisfactory energy dissipation and hysteresis behavior, eliminating the need for code limitations. The hybrid frame exhibited increased ductility and resilience. Rai et al. (2013) compared conventional braced frames (OCBF) and aluminum shear-link enabled frames (SLBF). SLBF frames showed less base shear, overturning moments, and floor acceleration but greater floor drifts. Shear links absorbed energy, enabling SLBF frames to withstand higher seismic loads. Rahnavard et al. (2020) propose a seismic resisting technique for reinforced concrete (RC) frame buildings using a combination of a rubber core and a U-shaped friction damping system. The hybrid damper, composed of steel and aluminum elements, exhibits improved stability and increased energy dissipation capacities compared to the original RC frame. Ferraioli et al. (2023) applied metallic yielding dampers to an RC school building in Italy. Detailed investigations, seismic performance assessment, and design procedures were conducted. The effectiveness of the design approach was demonstrated through nonlinear response history analysis. The retrofit project's construction phases, costs, and execution timing were discussed. Khoshkalam et al. (2022) reviewed various yielding dampers proposed for improving seismic performance in structures. They focused on ADAS dampers, which experience strain localization and unexpected tensile axial forces. To address these issues, they proposed a modified ADAS damper with improved boundary conditions. They developed an equation to determine maximum shear stress using the Abaqus program and parametric study. Results showed that the MADAS damper had a 30% increase in force level in the nonlinear range compared to ADAS dampers. Additionally, MADAS dampers exhibited greater energy dissipation in large deformations. Zahrai and Mortezagholi (2018) explored the advantages of yielding dampers in seismic energy control and proposed a novel method for designing two types of yielding elliptical dampers. Finite element modeling and pushover analysis were conducted to assess their performance. The modified damper demonstrated improved efficiency in energy dissipation and equivalent viscous damping, making it easier to fabricate. Kothapalli et al. (2022) evaluated the effectiveness of concentric hollow circular steel bracings and hybrid metallic yield dampers as retrofitting techniques for severely damaged RC portal frames. They also assessed a specially designed coupler-box assembly for retrofitting damaged columns. The retrofitted frames showed significantly enhanced lateral load and deformation capacities, with a comprehensive increase of 2.0 times in braced frames and 2.5 times in damper-equipped frames compared to the bare frame. The retrofitted frames exhibited stable and symmetric post-yield behavior, surpassing the FEMA code guidelines for collapse prevention drift levels. Choi et al. (2023) examined hybrid rings combining SMA and steel for smart dampers. Pure SMA rings showed excellent recentering capacity. Outer steel rings enhanced energy dissipation slightly, reducing recentering, while inner steel

rings greatly increased damping but lost recentering. Loose connections are essential for maintaining recentering capacity. MirzaGoltabar Roshan et al. (2018) investigated the effectiveness of steel accordion dampers in enhancing the blast resistance of steel frames. Non-linear dynamic analysis using ABAQUS software evaluated single-span frames (1 and 4 stories) subjected to varying blast loads. Results indicated significant displacement reduction with accordion dampers, up to 98% at column tops during intense blasts for 1-story frames and up to 64% at the fourth story for 4-story frames. Gorji Azandariani et al. (2020b) analyze the energy absorption of a steel dual-ring damper through analytical and numerical studies, focusing on moment plastic hinge formation in steel rings. They establish relationships for yield strength, displacement, and elastic stiffness, validated by parametric FE studies and experimental data. They highlight increased energy dissipation with larger steel ring diameters and reduced ductility with higher D/t ratios.

Naseri et al. (2020) address the vulnerability assessment and strengthening of RC box-girder bridges post-earthquakes. Their study develops fragility curves using analytical methods, considering soil-abutment-pile interaction and strengthening techniques like steel jacketing and FRP layers. Nonlinear dynamic analyses on a three-span bridge reveal reduced median fragility with comprehensive seismic factors, highlighting effective pier strengthening methods. Cheraghi et al. (2024b) explored the seismic behavior of steel structures, focusing on Reduced Beam Section connections. Thirty numerical analyses in ABAQUS examined connections with flange holes and yield rings in beam configurations. Equations for maximum moment strength and beam behavior were developed. Results show SRD connections offer significantly higher ductility and elastic stiffness than Reduced Beam Section models under axial forces. In other studies, different types of damper geometries have been investigated alone, which can be mentioned as U-shaped (Cheraghi et al., 2023b), steel ring dampers (SRDs) (Gorji Azandariani et al., 2020a), angled u-shape (Cheraghi et al., 2024a, 2024c), ADAS (Cheraghi et al., 2024d), and Bar Damper (Ghaedi et al., 2021).

In this research, a parametric study was conducted to investigate the effect of the SRD on the concrete frame, an aspect that has not been previously investigated. Firstly, the numerical model was calibrated using two samples of the experimental model. Subsequently, the influence of the radius and thickness of the SRD on the stiffness, ductility, strength, and energy dissipation parameters of the RC frame was examined. Additionally, approximate equations were formulated based on the curve fitting technique, enabling the calculation of the frame's stiffness and strength. Lastly, the most influential parameters on the results were identified.

In previous studies, the suggested location of the yield damper is illustrated in Figure (1) (Bagheria et al., 2011; Ebadi Jamkhaneh et al., 2019; Maleki & Mahjoubi, 2013; Zheng et al., 2015). It is observed that when a lateral force is applied to the frame, the change in the length of the spring is equal to the lateral displacement of the frame. According to the law of parallel springs, the force is distributed between the frame and the damper in proportion to their respective elastic stiffness (as described by Equations (1) and (2)) (Hibbeler & Tan, 2006). In these two equations, K_{Damper} and K_{Frame}, respectively, denote the stiffness of the dampers and the lateral stiffness of the frame. Thus, it is crucial to carefully adjust the stiffness ratio between the damper and the frame to design such structures. This research conducted a precise evaluation of this stiffness ratio on the parameters. It should be noted that in previous studies, the effect of SRD on steel frames has not been investigated, which contributes to the novelty of this research.

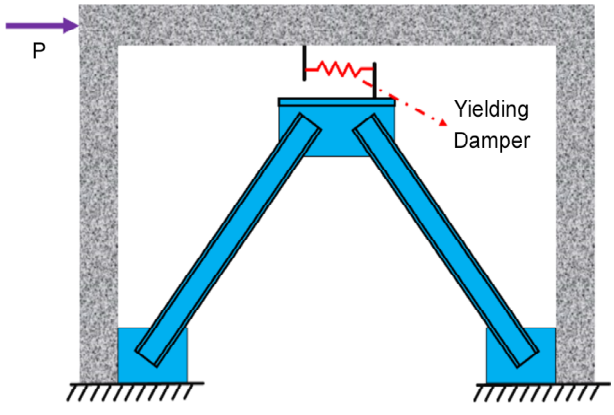

Figure 1. Schematic model of an RC frame equipped with a yielding damper.

$$F_{Damper} = \frac{K_{Damper}}{K_{Damper} + K_{Frame}} P \quad (1)$$

$$F_{Frame} = \frac{K_{Frame}}{K_{Damper} + K_{Frame}} P \quad (2)$$

2. Verification of Numerical Model

Since the experimental study of a concrete frame equipped with an SRD has not been conducted previously, two experimental samples were utilized to calibrate the numerical model. These samples include a bare RC frame and an SRD, which are presented separately in the following.

2.1. Verification of the Concrete Frame

To calibrate the concrete frame model, the experimental studies conducted by Tahamouli-Roudsari et al. (2019b) were utilized. The schematic of their model is presented in Figure (2). This concrete frame scaled 1:3, was examined in the laboratory. The frame was bolted to the experimental floor using 12 bolts, which prevented damage to the base of the column and rotation at the connection area. This experimental frame is loaded laterally.

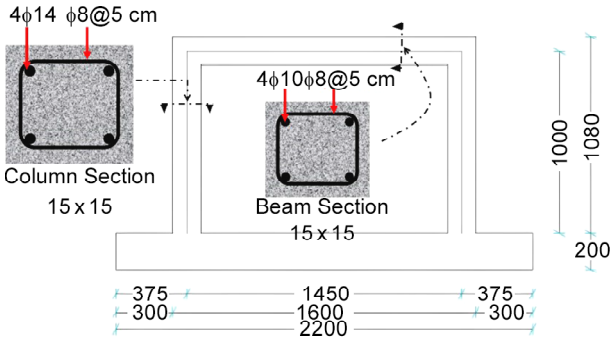

Figure 2. Dimensions of the experimental model (units: mm) (TahamouliRoudsari et al., 2019b).

The numerical modeling in this study was conducted using ABAQUS software. The numerical modeling of the experimental frame was performed based on the following assumptions:

- The concrete and rebars were modeled using solid (C3D8R) and truss (T3D2) elements.
- The numerical model incorporated the strain hardening effect and geometric and material nonlinearities and accounted for large deformations. The analysis was conducted using a displacement-control approach and the Static General solver.
- Sensitivity analysis of the results determined that the mesh dimensions for concrete and rebars were 30 mm.
- The modeling of the foundation was neglected since there was no evidence of rotation or damage reported in connecting the column to the foundation in the experimental model by (TahamouliRoudsari et al., 2019b).
- In the numerical model, concrete damage in tension and compression was considered using Equation (3), with concrete stress (f_c) and strength (σ_c) (ABAQUS, 2014).
- The Concrete Damage Plasticity (CDP) was employed to model the concrete, with specifications based on the ABAQUS documentation and presented in Table (1).

Table 1. Suggested values for CDP (Hibbitt, 2014).

Dilation Angel	Eccentricity	F_{b0}/f_{c0}	K	Viscosity Parameter
34	0.1	0.16	0.667	0.001

The stress-strain diagram for concrete in compression and tension was defined according to the guidelines in Eurocode 2 (Eurocode2, 2004), using Equation (4) and depicted in Figure (3a). The compressive strength of concrete (σ_{cu}) was reported as 38.3 MPa (TahamouliRoudsari et al., 2019b), and the corresponding strain values for maximum strength (ε_{c1}) and ultimate strain (ε_{cu1}) were calculated as 0.0022 and 0.0035, respectively. The Young's modulus of concrete (E_c) was suggested to be 34660 MPa. The stress-strain diagram for concrete and rebars was defined as depicted in Figures (3b) and (3c). The parameters used in Equation (4) are introduced in Equations (5) and (6).

$$d_c(\sigma_c) = \begin{cases} 0 \rightarrow if\ \sigma_c \leq f_c \\ 1 - \dfrac{\sigma_c}{f_c} \rightarrow if\ \sigma_c > f_c \end{cases} \quad (3)$$

$$\sigma = \sigma_{cu}(k\eta - \eta^2 / 1 + (k-2)\eta) \quad (4)$$

$$\eta = \varepsilon / \varepsilon_{c1} \quad (5)$$

$$k = 1.05 E_c \varepsilon_{c1} / \sigma_{cu} \quad (6)$$

Figure (4a) shows the meshed numerical model and its boundary condition. Following the analysis of the numerical model, the strain contour of the model

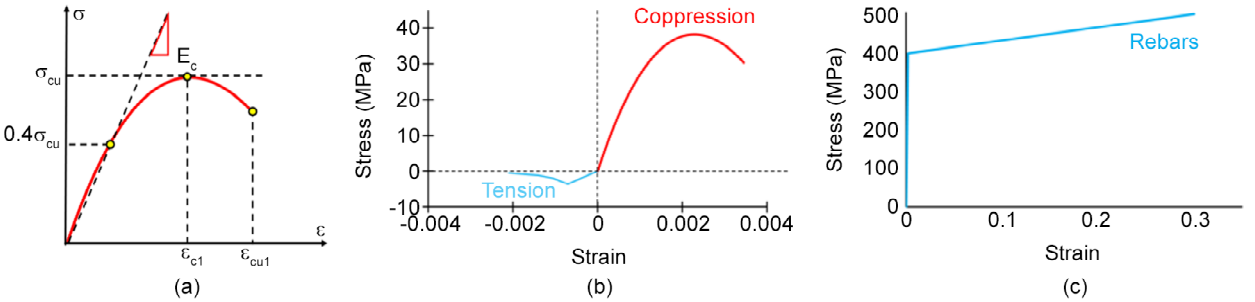

Figure 3. (a) Eurocode 2 proposal for concrete stress-strain diagram (Standard, 2004) (b) concrete strain stress curve in tension and compression and (c) the stress-strain curve of rebars.

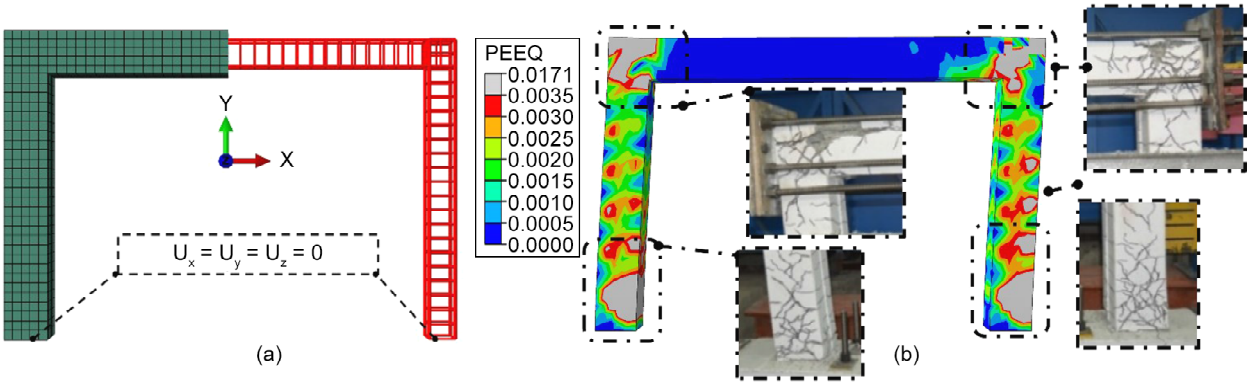

Figure 4. (a) FE model and its boundary condition and (b) Numerical model stress versus experimental failure (Tahamouli-Roudsari et al., 2019b).

was compared with the experimental results at the final moment, as depicted in Figure (4b). It can be observed that in the cracked regions of the experimental sample, the strain surpassed the ultimate limit of 0.0035. It shows that the failure mode of the numerical model is reasonably close to the experimental result.

After analyzing the numerical model, the force-displacement diagram of the numerical model was compared to the backbone diagram of the experimental model, as shown in Figure (5). It can be seen to more accurately compare numerical and experimental results, three important results, including final strength, elastic stiffness, and the area under the two diagrams, were calculated and compared with Table (2).

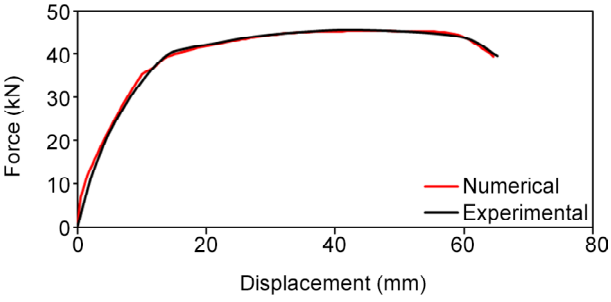

Figure 5. Force-displacement results of the numerical and experimental samples.

Table 2. Comparison of numerical and experimental results.

Parameters	FEM	Experimental
Elastic stiffness (kN/mm)	4.2	3.9
Ultimate strength (kN)	43.1	43.2
Energy dissipation (kN.mm)	2521.8	2587.1

2.2. Verification of SRD

To verify the accuracy of the numerical model of SRD, the experimental sample was conducted by Andalib et al. (2014) was utilized, as depicted in Figure (6a). Due to the low thickness of the damper compared to its other dimensions, the shell element (S4R) was used for numerical modeling. The analysis of the model was conducted using a Static General solver.

As there were no reported failures in the connection and bolt area of the experimental model, the numerical model of the damper was simplified as a ring, as shown in Figure (6b). Through a sensitivity analysis, the mesh dimensions for the damper were determined to be 7.5 mm. The damper was then analyzed using the displacement-control technique, with a displacement of 14.2 mm applied to the damper. After analyzing the model, the stress contour at the end of the loading was compared to

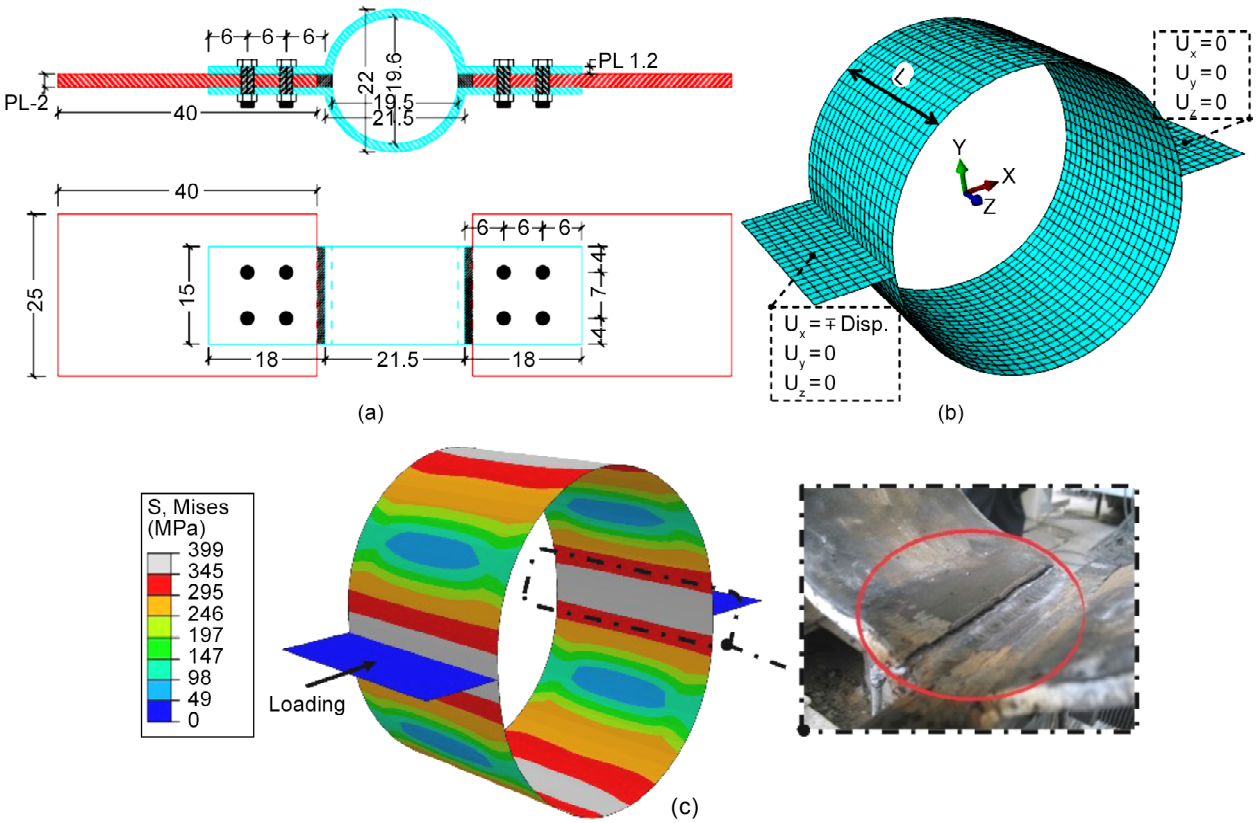

Figure 6. (a) Specifications of the experimental sample (Units: cm) and (b) numerical model and its boundary conditions (c) Numerical model stress versus experimental failure (Andalib et al., 2014).

the failure observed in the experimental model, as shown in Figure (6c). It is evident that the stress in the numerical model is highest at the point of force application, which corresponds to the damaged area in the experimental model. Because the behavior of the damper in tension and compression is almost the same. In the verification model and its effect on the concrete frame, it was assumed only in the compression mode.

Figure (7) shows the numerical model and experimental sample results. The numerical and experimental model results are close to each other with acceptable accuracy and can be used for further analysis.

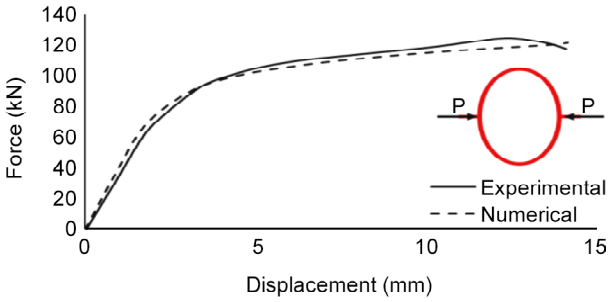

Figure 7. Comparison of numerical and experimental model results.

In a separate study, Equation (7) was proposed to calculate the elastic stiffness of the SRD (Gorji Azandariani et al., 2020a). This section also includes an analysis of yielding dampers with specifications listed in Table (3), similar to the verification sample. Upon analyzing the models outlined in Table (3), force-displacement diagrams were extracted, as depicted in Figure (8). The effective stiffness obtained from these diagrams was subsequently compared to the results derived from Equation (7) in Table (3), demonstrating a good agreement between the two results. In this equation, L, t, and r represent the length, thickness, and radius of the damper, respectively.

$$K_{e,SRD} = 945L\left(\frac{t}{2r}\right)^3 \text{ (kN / mm)} \quad (7)$$

3. Parametric Studies on SRD's Impact on RC Frames

In this section, the effect of SRD on the concrete frame was investigated. In the same way, the verified concrete frame with the same dimensions was equipped with SRD with the dimensions introduced in Table (3). Figure (9) illustrates the

model specifications and the dimensions of the sections utilized in it. The following points were considered in the design of this model:

- The dimensions of the braces were considered so that they do not buckle until the end of loading. The maximum force transmitted from a damper to a frame equals its ultimate strength. Therefore, this force must be utilized in the design of braces
- The damper was placed in the location experiencing the highest displacement.
- All the connections between steel parts, as well as the connection between steel and concrete members, were made with the "Tie" technique in the numerical model.

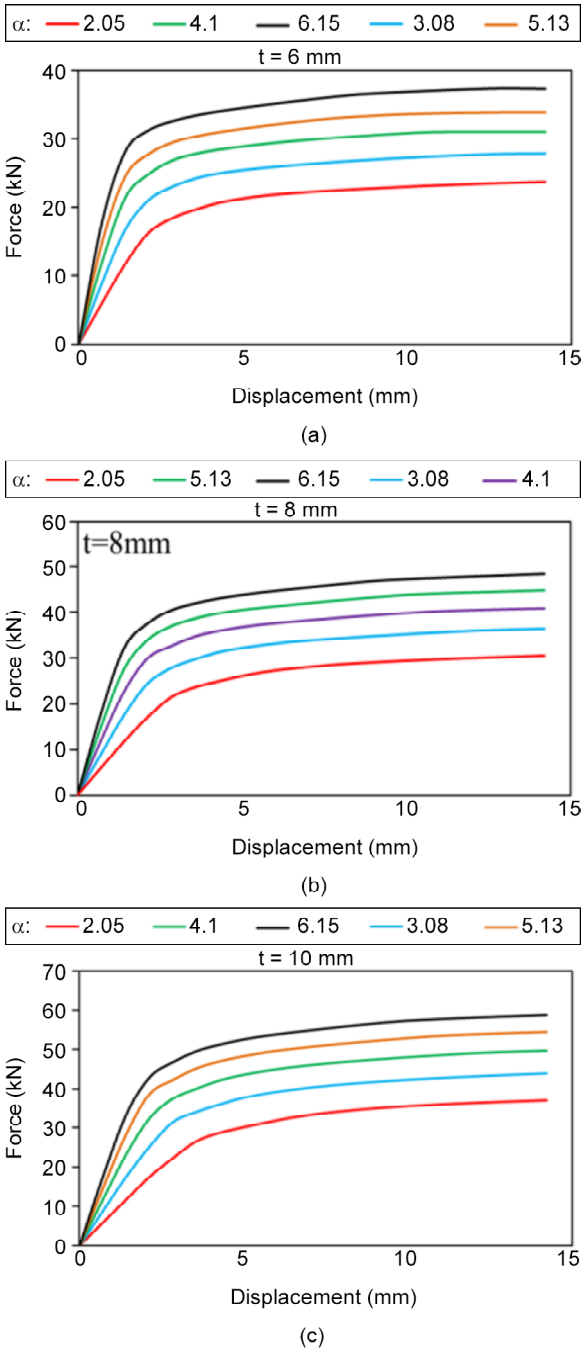

Figure 8. The results of the force-displacement diagram of the models in Table (3).

Table 3. Numerical models of SRD.

S-t- α	Dimensions of SRD (mm)			$K_{e,SRD}$ (kN/mm)		$\alpha = \frac{K_{e,SRD}}{K_{e,frame} = 3.9}$
	L	t	R	FEM	Eq. (7)	
S-6-2.05	100	6	68.3	8.22	8	2.05
S-6-3.08			59.7	11.97	12	3.08
S-6-4.1			54.2	15.67	16	4.10
S-6-5.13			50.3	19.02	20	5.13
S-6-6.15			47.4	23.29	24	6.15
S-8-2.05		8	91.1	8.11	8	2.05
S-8-3.08			79.6	12.18	12	3.08
S-8-4.1			72.3	16.03	16	4.10
S-8-5.13			67.1	19.77	20	5.13
S-8-6.15			63.2	23.43	24	6.15
S-10-2.05		10	113.9	8.13	8	2.05
S-10-3.08			99.5	12.02	12	3.08
S-10-4.1			90.4	16.07	16	4.10
S-10-5.13			83.9	20.06	20	5.13
S-10-6.15			79.0	23.65	24	6.15

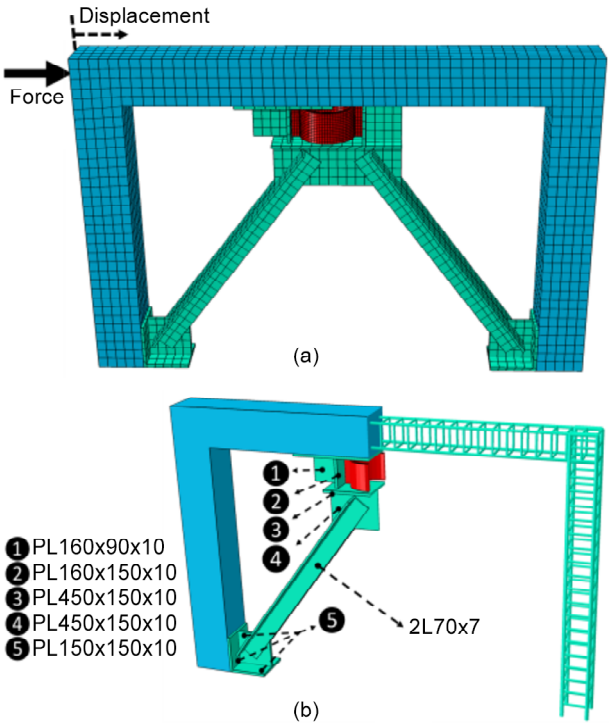

Figure 9. (a) The meshed model and the location of the applied forces (b) Details of the numerical model of RC frame equipped with SRD.

- Plates 1 and 2 in Figure (9b) should be designed to yield only at the end of loading.

This section analyzed the RC frame equipped with SRD using a displacement-control approach. Similarly, the models in this section were loaded until the curve dropped. The resulting nonlinear curve was then extracted, and a simplified bilinear diagram was generated based on FEMA 440 code (Fema, 2005), as depicted in Figure (10).

According to the instructions of this standard, the two-line diagram should be drawn so that the area under the two curves is equal and the two curves intersect at 0.6 of the yield force. The elastic stiffness and ductility were defined by Equations (8) and (9), and the energy dissipation was calculated as the area under the curve. The ultimate strength was determined by the force V_u. Additionally, Figure (11) presents four examples of the results of the models examined in this section, along with the corresponding bilinear diagrams.

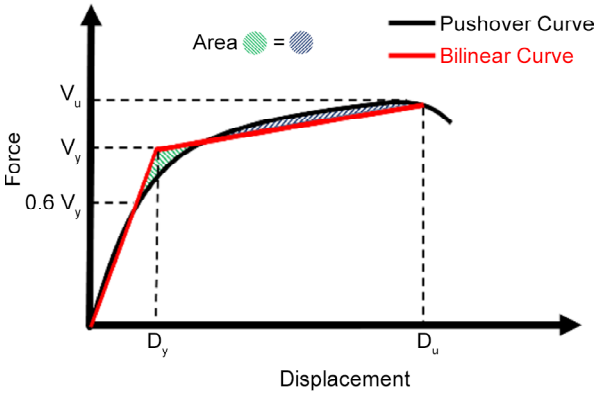

Figure 10. The nonlinear displacement-force diagram and its bilinear representation.

$$K_e = V_y / D_y \tag{8}$$

$$Ductility = D_u / D_y \tag{9}$$

3.1. Results of Parametric Studies

After obtaining the force-displacement diagrams and their corresponding bilinear diagrams, this section compares the parameters deduced from them, including stiffness, ultimate strength, ductility, and energy dissipation. Figures (12a) and (12b) display the results of the ultimate strength and elastic stiffness of the frame. These diagrams normalize the results to those of the bare frame. It can be observed that as "α" and the thickness of the damper increase, the ultimate stiffness and strength of the frame also increase. To calculate these parameters, curve fitting techniques were utilized, resulting in the introduction of Equations (10) and (11). Figure (12) also illustrates the results of these equations alongside the numerical results, demonstrating their close agreement with acceptable accuracy. It is important to note that the dimensions in these equations should be considered in "mm". In these two equations, K_{BF} and $V_{(u,BF)}$

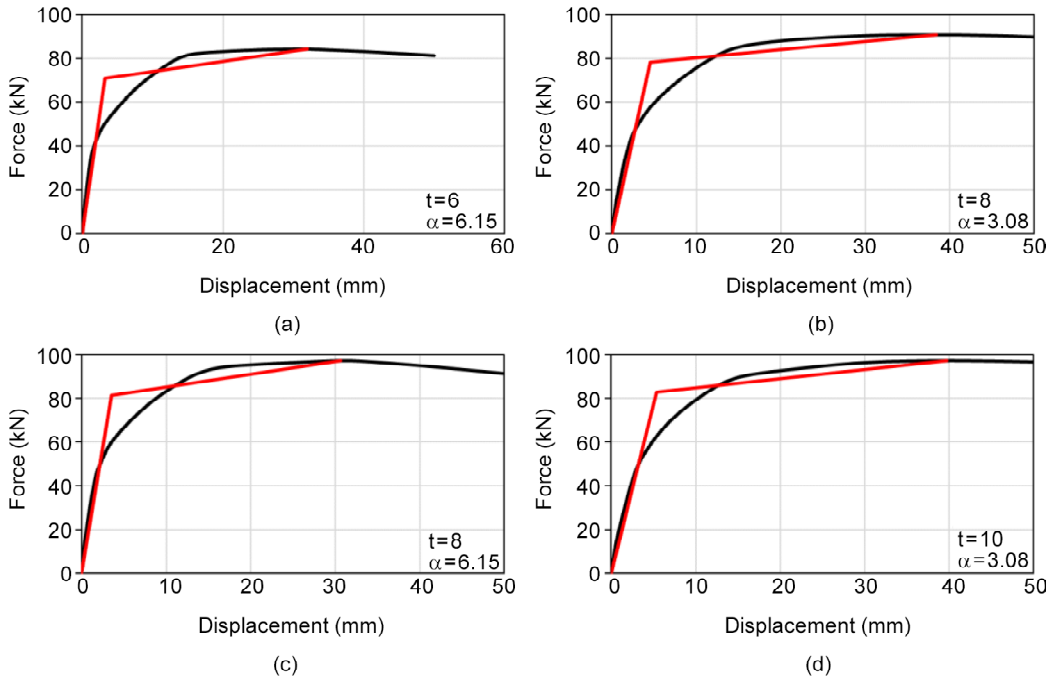

Figure 11. The results of concrete frames equipped with SRC with dimensions (a) S-6-6.15 (b) S-8-3.08 (c) S-8-6.15 and (d) S-10-3.08.

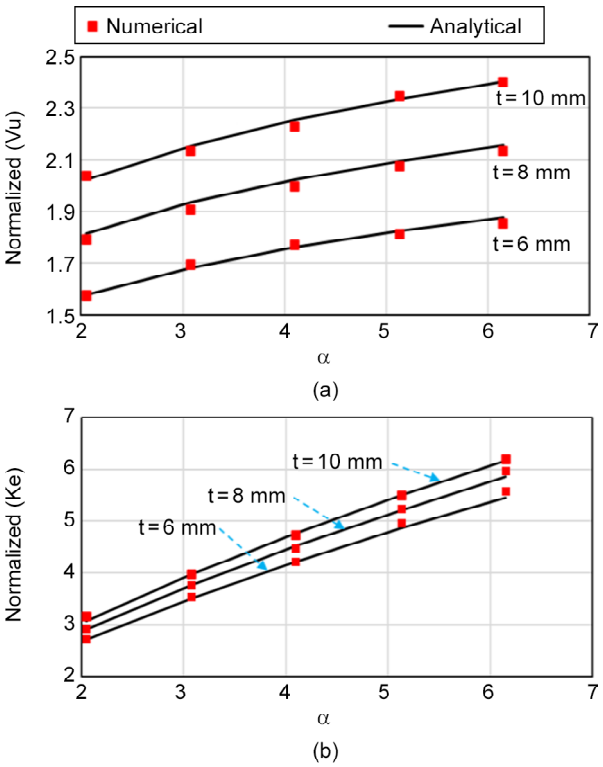

Figure 12. Results of (a) ultimate strength and (b) stiffness normalized to bare frame.

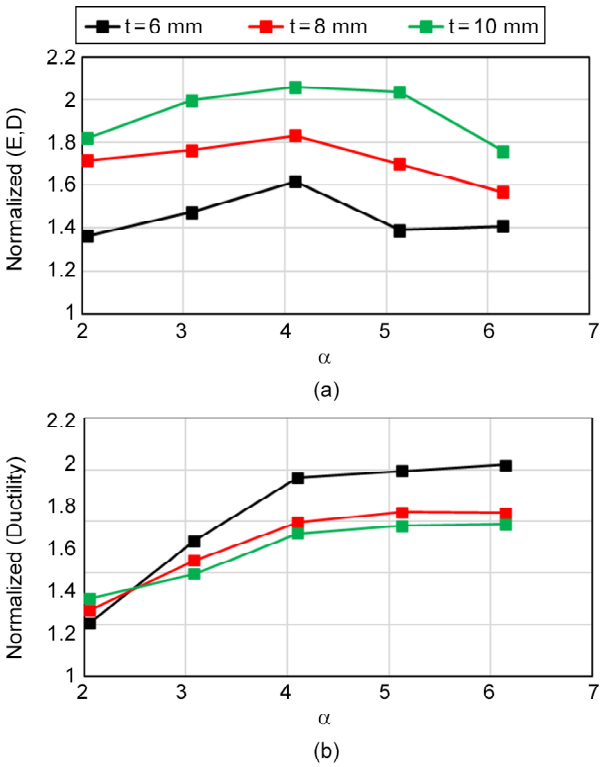

Figure 13. Normalized (a) energy dissipation and (b) ductility compared to the bare frame.

represent the ultimate stiffness and strength of the bare frame, which are reported as 3.9 kN/mm and 45.5 kN, respectively (TahamouliRoudsari et al., 2019b). It should be noted that the units considered for each of the dimensions of the damper in these equations must be in millimeters.

$$K_e = \left(180 \times \frac{t^{2.14}}{R^{1.9}}\right) K_{BF}\,(\text{kN/mm}) \tag{10}$$

$$V_u = \left(2 \times \frac{t^{0.95}}{R^{0.46}}\right) V_{u,BF}\,(\text{kN}) \tag{11}$$

Figure (13a) shows the normalized energy dissipation of the models to the bare frame. It is evident that increasing the thickness of the damper results in increased energy dissipation (E, D). Furthermore, when "α" is increased to 4.1, the energy dissipation is also increased, but then it starts to decrease. In the best case, the energy dissipation of the frame was two times that of the bare frame. In the models where the stiffness of the damper is high ($\alpha > 4.1$), a significant portion of the force is transferred to the damper. As a result, the damper yields quickly, and once it yields, the entire force is transferred to the frame, causing it to yield as well. On the other hand, when the force transmitted to the damper is more balanced ($\alpha < 4.1$), the damper will yield slightly later compared to the previous case. Consequently, the frame will yield after the damper yields.

Figure (13b) shows the normalized ductility. In contrast to the energy dissipation result, increasing the damper thickness reduces the ductility. However, increasing "α" up to 4.1 enhances the ductility of the frame, after which it remains constant.

In this study, investigations were conducted on a single-span, single-story frame. As observed in Table (3), models were considered based on the stiffness ratio of the damper to the frame. This allows for designing dampers compatible with the structure by adjusting them for different numbers of floors or varying frame stiffness. As seen in Figures (12) and (13), all results were presented based on the "α" coefficient, defined as the damper stiffness-to-lateral frame stiffness ratio. Thus, in taller buildings, one can first calculate the lateral stiffness of each floor and then design dampers accordingly. This technique has also been suggested in previous studies (TahamouliRoudsari et al., 2022, 2019a), where by calculating the stiffness ratio of the damper to the floor stiffness, the optimal design can be achieved for such models.

4. Examining the Magnitude of Variable Impact on Results

In the previous section, it was observed that each of the variables of the model had a different effect on the seismic parameters of the concrete frame. For this reason, it is essential to identify the influencing parameters on each parameter. For this purpose, the main effect diagrams were presented in the form of Figure (14), which shows the magnitude of the effect of the damper thickness and "α" on stiffness, ultimate strength, ductility, and energy dissipation. The vertical axis of these figures shows the average of all results. In these diagrams, the presence of a main effect can be determined if the line is not horizontal. Additionally, a steeper slope of the line corresponds to a greater magnitude of the main effect. Also, if the slope of the curve is positive, that is, with the increase of that variable, the results will increase (Evans, 2009). According to these diagrams, the following results can be expressed:

- The effect of "α" on the stiffness of the frame has been greater than the thickness of the damper. The thickness of the damper on the ultimate strength is greater than "α".
  The slope of the "α" curve in energy dissipation and ductility was positive up to 4.1, and then it was negative and almost zero.
- By comparing the four results, it becomes apparent that the damper thickness had the most negligible impact on the stiffness of the frame. Also, the effect of the damper thickness on the energy dissipation is greater than the ductility of the frame, even though the slope of the curve is positive in one and negative in the other.
- If "α" changes from 2.05 to 4.1, the effect of damper thickness on frame ductility is more than that of radius.

5. Failure Mechanism in Models

The concrete frame mechanism is equipped with SRD when the plastic hinges in the frame and damper are shown in Figure (15). In this case, the stiffness of the model is equal to zero, and the force-displacement curve starts to decrease according to Figure (11).

Considering the similarity in the mechanics of all the models, Figure (16) displays the contour of plastic strain and Von-Mises stress of one of the models. The Von-Mises stress can be calculated using Equation (12). The plastic strain contour (Figure 16a) reveals that the concrete strain has surpassed the ultimate strain (0.0035) at four points of the frame. Furthermore, based on the stress contour (Figure 16b), it can be observed that the SRD has yielded at four points, leading to

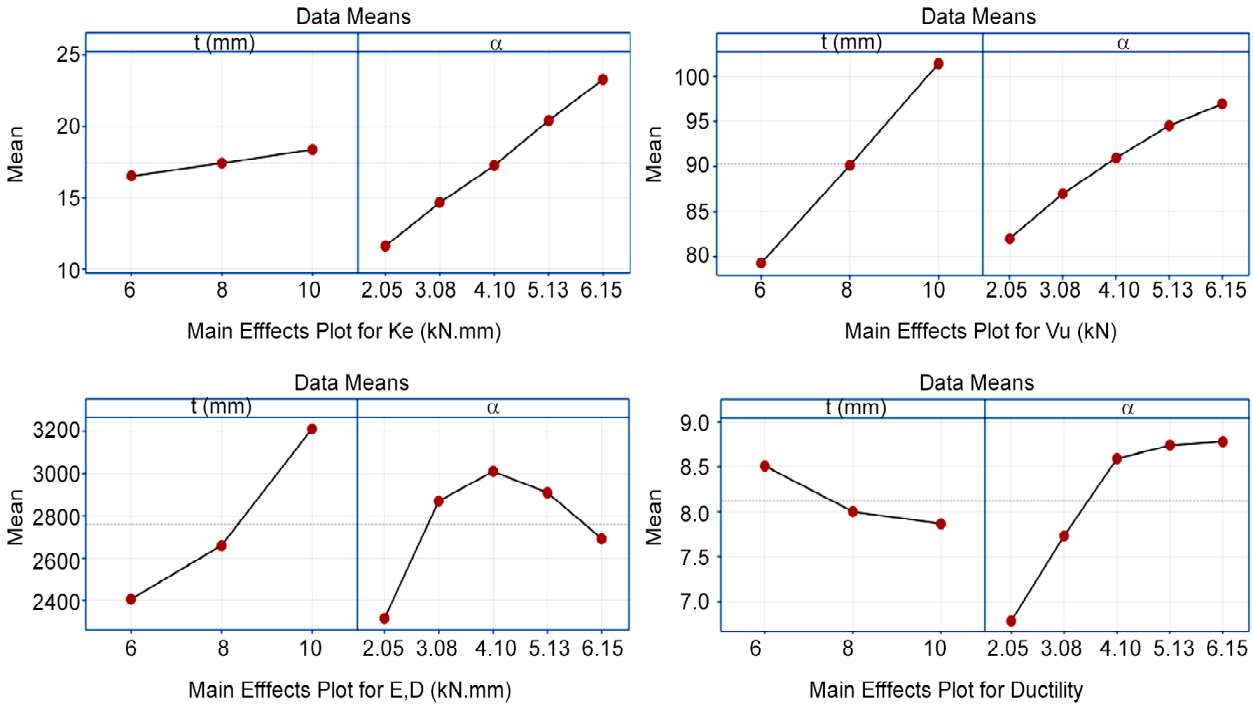

Figure 14. Main effect plots for stiffness, ultimate strength, energy dissipation, and ductility.

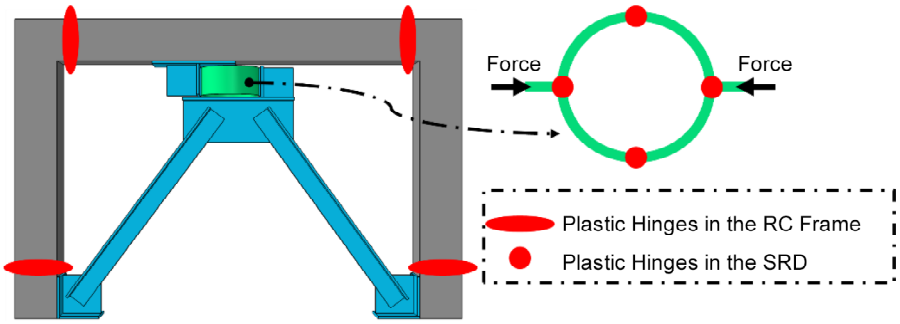

Figure 15. Locations of plastic hinge formation in the frame equipped with SRD.

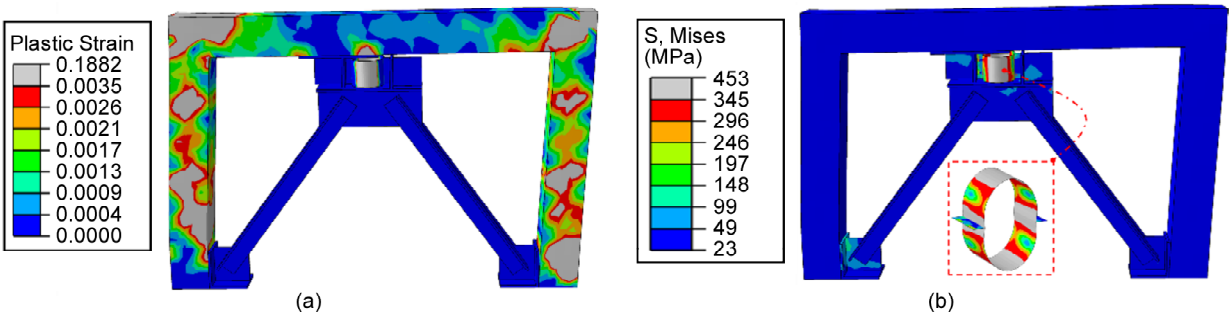

Figure 16. The contour of (a) plastic strain and (b) Von-Mises stress at the moment of mechanism.

Table 4. Specifications of earthquake records.

No. of Rec	Event	Year	Mag	Mechanism	R_{jb} (km)
Rec1	Mammoth lakes-01	1980	4.94	Normal oblique	12.56
Rec2	Morgan hill	1984	6.19	Strike slip	12.06
Rec3	Palm springs	1986	6.06	Reverse oblique	12.79
Rec 4	Northridge-01	1994	6.69	Reverse	12.42
Rec 5	Northridge-01	1994	6.69	Reverse	10.31
Rec 6	Parkfield-02, ca	2004	6.0	Strike slip	12.29
Rec 7	Northridge	1994	6.7	Thrust	10.1

the mechanism of the model. Additionally, none of the connection plates have yielded and the braces have not buckled, indicating the correctness of their dimension calculation.

$$\sigma_v = \sqrt{\frac{1}{2}\left[(\sigma_{11}-\sigma_{22})^2+(\sigma_{22}-\sigma_{33})^2+\sqrt{(\sigma_{33}-\sigma_{11})^2}\right]+3(\sigma_{12}^2+\sigma_{23}^2+\sigma_{13}^2)^2} \quad (12)$$

6. Dynamic Behavior of the Frame Equipped with SRD

In this section, the dynamic behavior of a frame equipped with a yielding damper was investigated. For this purpose, model S-10-5.13 was examined due to its superior performance in energy dissipation and ductility. All specifications of the model were considered similar to those in Section 3, with the distinction that dynamic analysis was conducted. Accordingly, dynamic analysis using the dynamic implicit was employed. Earthquake records used for dynamic analysis are introduced in Table (4).

After performing the dynamic analysis, the displacement of the frame with and without the damper was compared. Following the dynamic analyses, the displacement of the frame was computed, with the results presented in Figure (17). To facilitate a more effective comparison of the outcomes, the maximum absolute displacement was calculated.

After calculating the absolute maximum displacement of the frame, the results are illustrated in Figure (18).

It is observed that in all models, the addition of dampers has resulted in a reduction in frame displacement. On average, the incorporation of dampers has led to a 60% decrease in frame displacement.

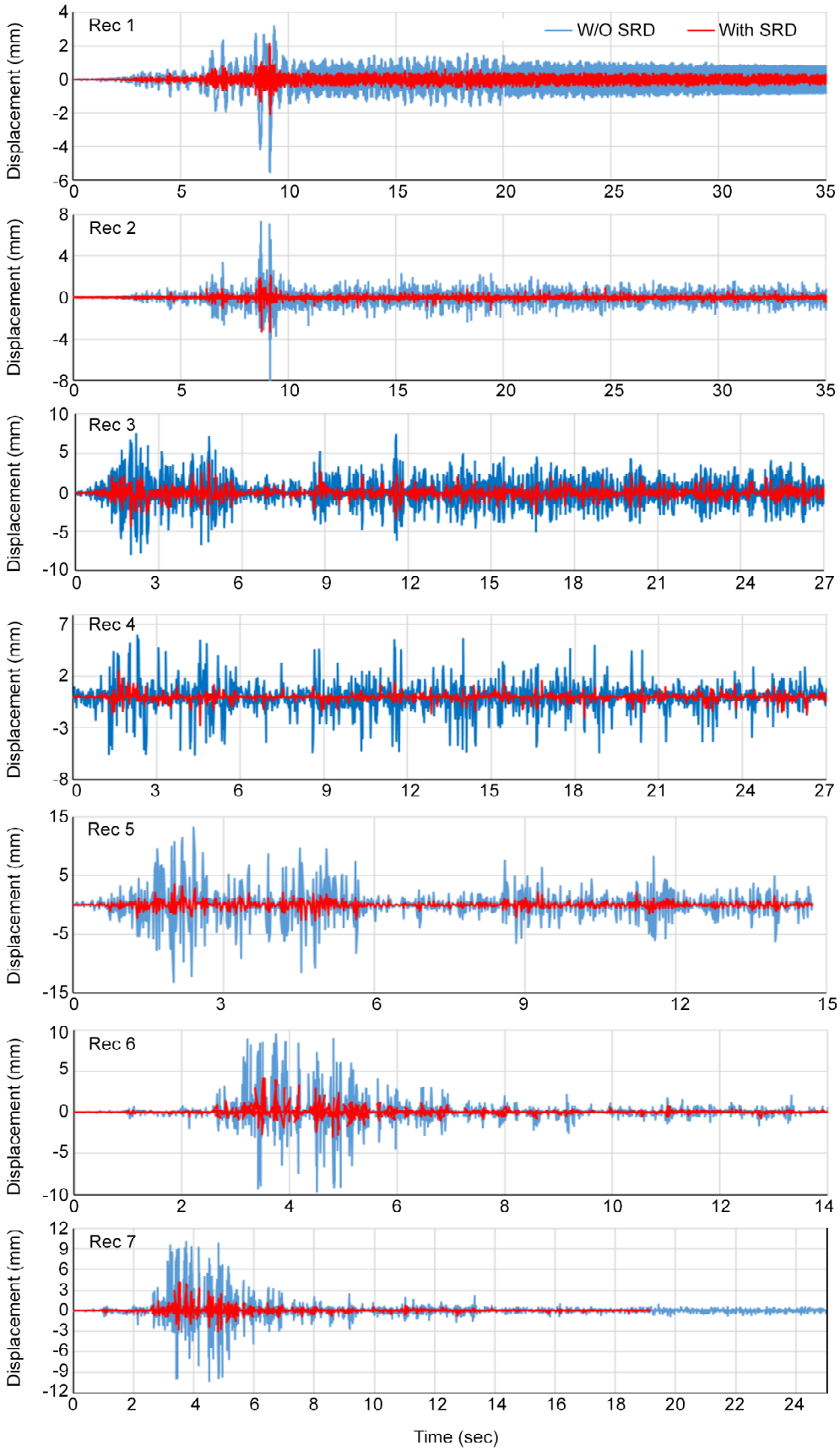

Figure 17. The history of displacement of the frame under the earthquakes introduced in Table (4).

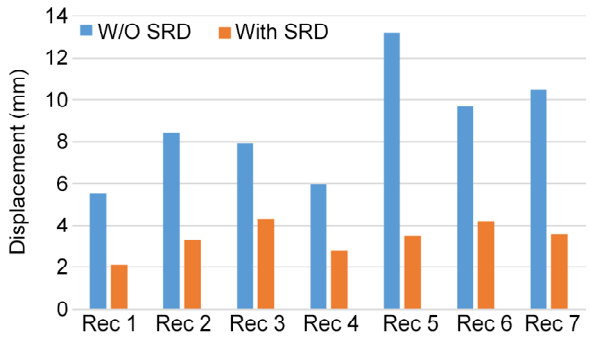

Figure 18. Maximum displacement of the frame.

7. Conclusion

In this study, the impact of SRD on a concrete frame was examined through numerical analysis. Two experimental samples were employed to calibrate the numerical model. Subsequent numerical analyses were performed using a push-over method on the SRD, and the stiffness derived from the numerical model was compared with an analytical equation, showing good agreement. Additionally, the effects of the damper's radius and thickness on the seismic behavior of the concrete frame were assessed. The analyses were conducted using nonlinear static methods, and the outputs of the model included stiffness, strength, energy absorption, and ductility. Also, the most influential variables of the model on these parameters were identified. Finally, the dynamic behavior of the frame equipped with dampers was examined under seven different earthquake scenarios. The results of the studies can be summarized as follows:

- Increasing the damper's thickness and reducing its radius enhances the frame's stiffness and ultimate strength. The relationship between these parameters and "α" shows a nearly linear increase. Also, the approximate equations proposed to calculate these two parameters of the concrete frame agreed with the numerical results.
- Increasing the damper's thickness enhances energy dissipation but reduces the ductility of the RC frame. Moreover, increasing "α" up to 4.1 enhances energy dissipation and ductility of the RC frame. However, beyond 4.1, the rate of energy dissipation and ductility of the concrete frame remains constant. Also, when the stiffness ratio of the damper to the bare frame is set to 4.1, the energy dissipation and ductility of the concrete frame will be twice that of the bare frame.

  The parameter "α" has the greatest impact on the stiffness of the RC frame, while the damper thickness has the most significant influence on the ultimate strength. The damper thickness has the least effect on the stiffness of the frame. Furthermore, when "α" changes from 2.05 to 4.1, the influence of the damper thickness on the ductility of the frame becomes more pronounced.
- In concrete frames equipped with SRD, the stiffness ratio of the damper to the frame plays a crucial role in the seismic parameters of the frame. Additionally, when designing the plates connecting the damper to the frame, as well as the braces, it is important to consider that the forces applied to these members should be designed based on the maximum force from the damper to the frame.
- The results of the dynamic analyses indicated that the addition of dampers resulted in a 60% reduction in frame displacement.

References

Andalib, Z., Kafi, M. A., Kheyroddin, A., & Bazzaz, M. (2014). Experimental investigation of the ductility and performance of steel rings constructed from plates. *Journal of Constructional Steel Research*, *103*, 77-88. https://doi.org/10.1016/j.jcsr.2014.07.016

Bagheria, S., Hadidi, A., & Alilou, A. (2011). Heightwise distribution of stiffness ratio for optimum seismic design of steel frames with metallic-yielding dampers. *Procedia Engineering*, *14*, 2891-2898. https://doi.org/10.1016/j.proeng.2011.07.364

British Standards Institution. (2004). *Eurocode 2: Design of Concrete Structures-Part 1-1: General Rules and Rules for Buildings (BS EN 1992-1-1:2004).*

Cheraghi, K., Darbandkohi, M., TahamouliRoudsari, M., & Kiasat, S. (2023a). Seismic behavior of RC frames with partially attached steel shear walls: A numerical study. *Earthquakes and Structures*, *25*(6), 443-454. https://doi.org/10.12989/eas.2023.25.6.443

Cheraghi, K., TahamouliRoudsari, M., & Kiasat, S. (2023b). Numerical and analytical investigation of

U-shape dampers and its effect on steel frames. *Structures*, *55*, 498-509. https://doi.org/10.1016/j.istruc.2023.06.037

Cheraghi, K., TahamouliRoudsari, M., Kiasat, S., & Cheraghi, K. (2023c). Numerical study of metallic dampers' effect on seismic performance of concrete frames. *Asian Journal of Civil Engineering*. https://doi.org/10.1007/s42107-023-00917-6

Cheraghi, K., Tavana, M. H., & Aghayari, R. (2023d). Investigating the effect of low-yield yielding dampers on the seismic behavior of steel frames. *Periodica Polytechnica Civil Engineering*, *67*(3), 925-933. https://doi.org/10.3311/PPci.21804

Cheraghi, K., TahamouliRoudsari, M., Kiasat, S., & Cheraghi, K. (2024a). Numerical and analytical investigation of cyclic behavior of D-shape yielding damper. *Structural Engineering and Mechanics*, *89*(4), 411. https://doi.org/10.12989/sem.2024.89.4.411

Cheraghi, K., TahamouliRoudsari, M., Kiasat, S., & Cheraghi, K. (2024b). Numerical and analytical investigation of reduced beam section with yielding damper and their comparison. *Journal of Seismology and Earthquake Engineering*, *26*(1), 31-45. https://doi.org/10.48303/jsee.2024.2010550.1072

Cheraghi, K., TahamouliRoudsari, M., Kiasat, S., & Esfandiari, J. (2024c). Numerical investigation of cyclic behavior of angled U-shaped yielding damper on steel frames. *Periodica Polytechnica Civil Engineering*, *68*(2), 426-434. https://doi.org/10.3311/PPci.23213

Cheraghi, K., TahamouliRoudsari, M., Kiasat, S., & Esfandiari, J. (2024d). Numerical and analytical study of the cyclic behavior of ADAS damper and the effect of axial force on its behavior. *Journal of Earthquake Engineering*, 1-18. https://doi.org/10.1080/13632469.2024.2345821

Choi, E., Nhan, B. T., & Ostadrahimi, A. (2023). On the performance of a smart hybrid damper consisting of shape memory alloy and steel rings. *Engineering Structures*, *291*, Article 116382. https://doi.org/10.1016/j.engstruct.2023.116382

Dassault Systèmes Simulia Corp. (2014). *ABAQUS 6.14 Analysis User's Guide (Vols. 1-3)*.

Ebadi Jamkhaneh, M., Ebrahimi, A. H., & Shokri Amiri, M. (2019). Experimental and numerical investigation of steel moment resisting frame with U-shaped metallic yielding damper. *International Journal of Steel Structures*, *19*(3), 806-818. https://doi.org/10.1007/s13296-018-0166-z

Evans, M. (2009). *MINITAB manual for David Moore and George McCabe's Introduction to the Practice of Statistics*. W. H. Freeman and Company.

Federal Emergency Management Agency. (2005). Improvement of nonlinear static seismic analysis procedures (FEMA 440). https://www.atcouncil.org/images/FEMA440.pdf

Ferraioli, M., Lauro, G. D., Crisci, P., Laezza, G., Lavino, A., & Bellantoni, C. (2023). Seismic retrofit of a RC building using metallic yielding dampers: A case study. *Procedia Structural Integrity*, *44*, 982-989. https://doi.org/10.1016/j.prostr.2023.01.127

Ghaedi, K., Ibrahim, Z., Javanmardi, A., & Rupakhety, R. (2021). Experimental study of a new bar damper device for vibration control of structures subjected to earthquake loads. *Journal of Earthquake Engineering*, 25(2), 300-318. https://doi.org/10.1080/13632469.2018.1515796

Gorji Azandariani, M., Abdolmaleki, H., & Gorji Azandariani, A. (2020a). Numerical and analytical investigation of cyclic behavior of steel ring dampers (SRDs). *Thin-Walled Structures*, *151*, Article 106751. https://doi.org/10.1016/j.tws.2020.106751

Gorji Azandariani, M., Gorji Azandariani, A., & Abdolmaleki, H. (2020b). Cyclic behavior of an energy dissipation system with steel dual-ring dampers (SDRDs). *Journal of Constructional Steel Research*, 172, Article 106145. https://doi.org/10.1016/j.jcsr.2020.106145

Hibbeler, R. C., & Tan, K.-H. (2006). *Structural Analysis (6th Ed.)*. Pearson Prentice Hall.

Hosseini Hashemi, B., & Keykhosrokiany, B. (2019). Buckling response and elastic stiffness of butterfly dampers. *Journal of Seismology and Earthquake Engineering*, *21*(4), 11-20. https://doi.org/10.48303/jsee.2019.243312

Khoshkalam, M., Mortezagholi, M. H., & Zahrai, S.

M. (2022). Proposed modification for ADAS damper to eliminate axial force and improve seismic performance. *Journal of Earthquake Engineering*, *26*(10), 5130-5152. https://doi.org/10.1080/13632469.2020.1859419

Kothapalli, N. K., Chidambaram, R. S., & Agarwal, P. (2022). Experimental evaluation of steel bracings and metallic yield damper as retrofit techniques for severely damaged RC building frames. *Journal of Earthquake Engineering*, *27*(12), 3564-3587. https://doi.org/10.1080/13632469.2022.2141373

Mahmoudi, F., Dolatshahi, K. M., Mahsuli, M., Nikoukalam, M. T., & Shahmohammadi, A. (2019). Experimental study of steel moment resisting frames with shear link. *Journal of Constructional Steel Research*, *154*, 197-208. https://doi.org/10.1016/j.jcsr.2018.11.027

Maleki, S., & Mahjoubi, S. (2013). Dual-pipe damper. *Journal of Constructional Steel Research*, *85*, 81-91. https://doi.org/10.1016/j.jcsr.2013.03.004

Mirzagoltabar Roshan, A., Naseri, A., & Nasiri Larimi, J. (2018). Investigating the effect of accordion thin walled dampers on reducing the response of frames subjected to blast loading. *Amirkabir Journal of Civil Engineering*, *49*(4), 707-722. https://doi.org/10.22060/ceej.2016.855

Naseri, A., Roshan, A. M., Pahlavan, H., & Amiri, G. G. (2020). Probabilistic seismic assessment of RC box-girder bridges retrofitted with FRP and steel jacketing. *Coupled Systems Mechanics*, *9*(4), 359-379. https://doi.org/10.12989/csm.2020.9.4.359

Rahnavard, R., Rebelo, C., Craveiro, H. D., & Napolitano, R. (2020). Numerical investigation of the cyclic performance of reinforced concrete frames equipped with a combination of a rubber core and a U-shaped metallic damper. *Engineering Structures*, *225*, Article 111307. https://doi.org/10.1016/j.engstruct.2020.111307

Rai, D. C., Annam, P. K., & Pradhan, T. (2013). Seismic testing of steel braced frames with aluminum shear yielding dampers. *Engineering Structures*, *46*, 737-747. https://doi.org/10.1016/j.engstruct. 2012.08.027

Sedaghatnezhad, H., Fallah, A., & Mosalman Yazdi, M. (2021). Probabilistic seismic demand assessment of chevron bracing steel moment frames with TADAS damper. *Journal of Seismology and Earthquake Engineering*, *23*(4), 51-66. https://doi.org/10.48303/jsee.2023.1987344.1045

TahamouliRoudsari, M., Cheraghi, K., & Aghayari, R. (2022). Investigating the retrofit of RC frames using TADAS yielding dampers. *Structural Durability & Health Monitoring*, *16*(4), 343-359. https://doi.org/10.32604/sdhm.2022.07927

TahamouliRoudsari, M., Cheraghi, K., & Habibi, M. R. (2019a). Investigation of retrofitting RC moment resisting frames with ADAS yielding dampers. *Asian Journal of Civil Engineering*, 20(1), 125-133. https://doi.org/10.1007/s42107-018-0092-6

TahamouliRoudsari, M., Torkaman, M., Entezari, A. R., Rahimi, H., & Niazi, K. K. (2019b). Experimental investigation of strengthening reinforced concrete moment resisting frames using partially attached steel infill plate. *Structures*, *19*, 173-183. https://doi.org/10.1016/j.istruc.2019.01.009

Zahrai, S. M., & Heisami, A. (2017). Seismic performance of tall buildings with impact damper under near and far-field earthquakes. *Journal of Seismology and Earthquake Engineering*, *19*(4), 327-336.

Zahrai, S. M., & Mortezagholi, M. H. (2018). Cyclic performance of an elliptical-shaped damper with shear diaphragms in chevron braced steel frames. *Journal of Earthquake Engineering*, *22*(7), 1209-1232. https://doi.org/10.1080/13632469.2016.1277436

Zahrai, S. M., & Parsa, A. (2015). Effect of flange width of vertical link beam on cyclic behavior of chevron braced steel frames. *Journal of Seismology and Earthquake Engineering*, *17*(4), 281-292.

Zheng, J., Li, A., & Guo, T. (2015). Analytical and experimental study on mild steel dampers with non-uniform vertical slits. *Earthquake Engineering and Engineering Vibration*, *14*(1), 111-123. https://doi.org/10.1007/s11803-015-0010-9